

# Site Assessment and Layout Optimization for Rooftop Solar Energy Generation in Worldview-3 Imagery

Zeyad Awwad <sup>1,†</sup> , Abdulaziz Alharbi <sup>2</sup>, Abdulelah H. Habib <sup>2,\*</sup> and Olivier L. de Weck <sup>1,†</sup>

<sup>1</sup> Massachusetts Institute of Technology; zeyad@mit.edu; deweck@mit.edu

<sup>2</sup> King Abdulaziz City for Science and Technology

\* Correspondence: ahhabib@kacst.edu.sa

† Current address: Engineering Systems Laboratory, Department of Aeronautics and Astronautics, Massachusetts Institute of Technology

**Abstract:** With the growth of residential rooftop PV adoption in recent decades, the problem of effective layout design has become increasingly important in recent years. Although a number of automated methods have been introduced, these tend to rely on simplifying assumptions and heuristics to improve computational tractability. We demonstrate a fully automated layout design pipeline that attempts to solve a more general formulation with greater geometric flexibility that accounts for shading losses. Our approach generates rooftop areas from satellite imagery and uses MINLP optimization to select panel positions, azimuth angles and tilt angles on an individual basis rather than imposing any predefined layouts. Our results demonstrate that although several common heuristics are often effective, they may not be universally suitable due to complications resulting from geometric restrictions and shading losses. Finally, we evaluate a few specific heuristics from the literature and propose a potential new rule of thumb that may help improve rooftop solar energy potential when shading effects are considered.

**Keywords:** Solar energy, photovoltaics, geometric optimization, residential energy generation, image processing, object detection, urban analysis

**Citation:** Awwad, Z.; Alharbi, A.; Habib, A.H.; de Weck, O.L. Site Assessment and Layout Optimization for Rooftop Solar Energy Generation in Worldview-3 Imagery. *Remote Sens.* **2022**, *14*, 0. <https://doi.org/>

Received:

Accepted:

Published:

**Publisher's Note:** MDPI stays neutral with regard to jurisdictional claims in published maps and institutional affiliations.

**Copyright:** © 2022 by the authors. Submitted to *Remote Sens.* for possible open access publication under the terms and conditions of the Creative Commons Attribution (CC BY) license (<https://creativecommons.org/licenses/by/4.0/>).

## 1. Introduction

### 1.1. Background

According to the International Energy Agency (IEA), global photovoltaic energy generation capacity reached nearly 160 GWp in 2020 [1]. Recent growth has been largely driven by the accelerating adoption of rooftop PV, which grew to nearly 60 GWp in 2020. However, in practice, residential PV system design remains a largely manual process. A number of automated approaches have emerged in recent years, but due to the computational complexity of the full optimization problem, they typically rely on predefined layouts, such as parallel rows, or nonlinear neglect terms, such as shading. This paper describes a fully automated approach that employs 0.31-meter RGB Worldview-3 satellite imagery to identify rooftops and subsequently generate complex solar panel layouts with detailed energy estimates that dynamically account for shading between panels during the optimization process.

As research into nonlinear optimization of multi-azimuth layouts with shading remains limited, we anticipate that the insights gained through this research will significantly contribute to the literature related to automated PV layout design.

The proposed approach detects rooftops automatically from high-resolution satellites using morphological image processing methods. We use rooftop geometries to define a set of candidate panel locations and compute their expected energy generation. Next we run a detailed geometric optimization that considers panel shading interactions to more accurately estimate energy generation and profit in a net metering scenario. Our analysis suggests that including these features in the optimization plays a significant role in site

assessment and layout design, and may assist in improving solar potential through insights into the role of building design and urban layouts.

### 1.2. Literature Review

A small but growing body of work has examined the automated design of rooftop PV systems. Several commercial tools can provide partially automated designs for rooftop PV systems based on simple predefined layout options, typically arranging panels in rows facing a single azimuth angle [2]. While these tools are undoubtedly valuable for aiding site analysis of a single rooftop, they often involve some degree of manual operation (such as drawing rooftop polygons and identifying obstacles). Such approaches also tend to be limited in the potential layouts they can generate without human intervention.

#### 1.2.1. PV Layout Design

Over the past few years, several academic groups have published work describing the use of remote sensing data and geometric optimization methods to automate the design of sophisticated rooftop layouts based on satellite and aerial data. Zhong et al used LIDAR data to detect and characterize rooftops and obstacles that interfere with panel placement [3]. Since their work primarily focused on sloped rooftops and panels mounted parallel to the roof surface, they presented a limited shading analysis from fixed sources such as the rooftop and surrounding structures (but not the interactions between nearby panels).

Similarly, recent work by Narjabadifam et al [4] employed 3D models from Google Maps as a starting point for optimizing the layout of rooftop PV systems. Their work included limited shading analysis between panels, considering the effect between parallel rows of panels along the same azimuth angle. While this approach can be effective for relatively large rooftops with few (or no) obstructions, it may not be suitable for complex rooftop geometries with significant obstructions. Rooftops with these properties are challenging for predefined layouts due to the geometric limitations of single-azimuth designs.

Despite these recent advances, several significant gaps still exist in the literature on the automated design of rooftop PV systems. The majority of existing work focuses on North American and European regions, which tend to feature homes with sloped roofs and commercial buildings with large and relatively open flat rooftops. In regions such as India and the Middle East, residential buildings typically have flat rooftops with partial storeys and numerous small obstructions such as air conditioning units and water tanks. These types of buildings are well suited to satellite image analysis since, aside from relative heights, most of its features are parallel to the image plane and do not require depth or slope information to analyze.

Additionally, current methods in the literature do not provide dynamic shading analysis of complex panel layouts. Due to challenges in both implementation and computational tractability, the implementations we reviewed often relied on heuristics designed for simple layouts such as parallel rows (which greatly simplify shading analysis) or neglected shading from neighboring panels entirely.

#### 1.2.2. Design Heuristics

In both manual and automated rooftop PV layout design, several recurring design heuristics and rules of thumb are used to improve baseline system performance for predefined layout templates. These recommended approaches generally serve to improve the desired property (e.g. individual panel generation, packing density) or reduce an undesirable property (e.g. shading between panels). However, to the best of our knowledge, these heuristics tend to be imposed on layout design methodologies and they haven't been shown to emerge naturally from optimization methods. Our study will evaluate whether these recommended design rules are consistent with the results of a full MINLP optimization.

One of the simplest and most universal recommendations is to start with azimuth and tilt angles that feature high energy generation potential [5]. For non-equatorial regions, this typically means equator-facing panels tilted approximately toward the sun during peak daylight hours. This rule becomes more complex in multi-panel systems since increasing the tilt angle also increases the area shaded by that panel. The resulting shading losses may outweigh any gains in baseline energy potential, so a simple greedy maximization may lead to poor total generation.

Another common approach is to use parallel row layouts with fixed spacing, which reduces shading losses and also provides easy maintenance access to all panels (a federal regulatory requirement in our region of study [6]). This layout is simple to implement and tends to generate effective results. Studies show a packing density of 0.7 (representing the ratio of total panel area to rooftop area) for simple spaced row layouts on typical American rooftops [5]. International studies have shown that the optimal spacing (and resulting density) depends on latitude since it should be selected to balance increased panel density with the loss in energy due to shading [7].

Additionally, in the broader context of general polygon packing problems, several methods rely on heuristics to improve packing density. A common heuristic is to align at least one edge of the packing object to one of the edges of the bounding shape (in our context, representing the solar panels and the rooftop polygon, respectively). This approach forms the basis of the "advancing front" packing algorithm [8] that only places new polygons in contact with the active front, representing the accessible edges of the existing polygons (either the bounding polygon or a previously placed object). Similarly, some geometric bin packing methods demonstrated that relying on mated edges tends to minimize wasted space and improve packing density [9]. However, heuristics that increase packing density need to be used carefully, since increasing panel density beyond the ideal spacing tends to diminish generation performance [7].

### 1.3. Contribution

The study described in this paper aims to address the gaps described above. Our optimization method does not impose predefined layouts and can generate multi-azimuth system designs to maximize energy generation after accounting for shading interactions. Additionally, we evaluate several heuristics and rules of thumb used in packing algorithms and automated rooftop PV layout design (such as single-azimuth equator-facing rows, and the relationship between panel and building orientation) and the potential role of urban planning in improving rooftop PV potential. The supporting results are generated from a fully automated method that relies on common high-resolution satellite imagery that targets flat rooftops with irregular geometries and obstacles, characteristic of buildings in the Middle East.

## 2. Materials and Methods

### 2.1. Overview

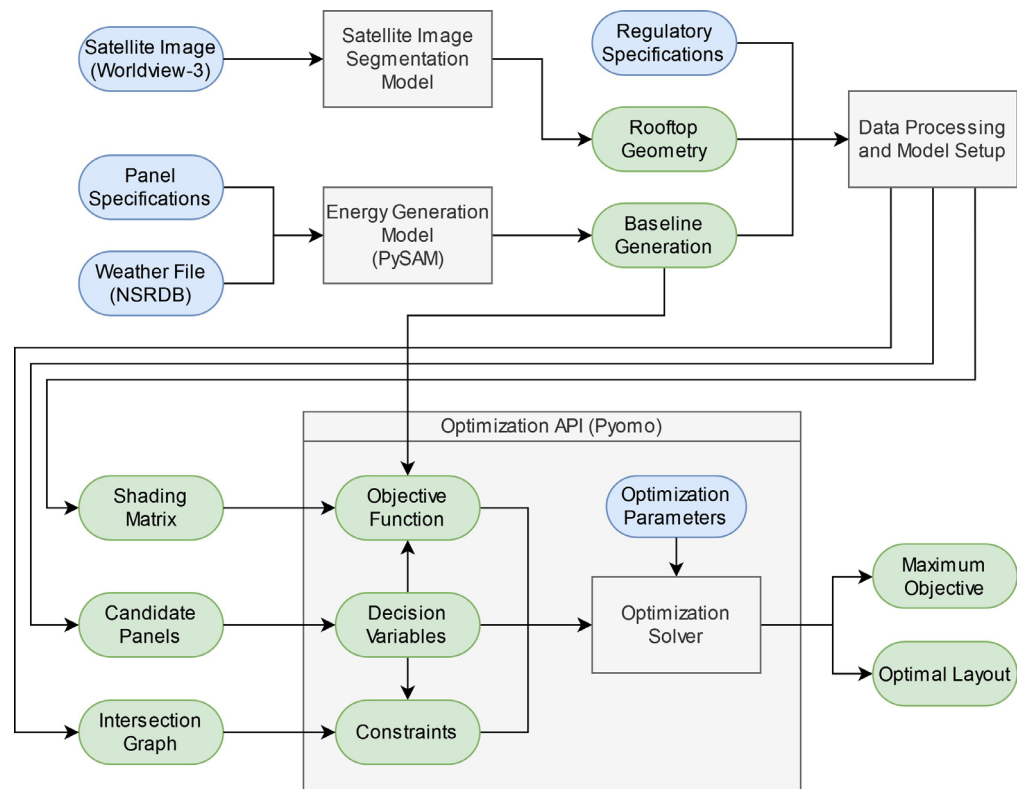
The optimization pipeline consists of several preprocessing steps that are used to define the rooftop geometry and candidate panels, along with the corresponding energy and shading profiles. These features are used to define a mixed-integer linear problem (MILP) or mixed-integer nonlinear problem (MINLP) model within Pyomo, a Python-based optimization API that provides a unified interface between many open-source and commercial solvers.

Aside from the user options, the primary data inputs are a 0.31-meter resolution satellite image and corresponding weather files for the geographic region. During preprocessing, we extract the rooftop area and detect potential obstacles from the satellite image to define a polygon for the optimization area (see 2.3.1). The rooftop geometry is used to filter the possible of candidate panels using an accept/reject procedure. We determine potential locations by overlaying dense grids of panels with different azimuth angles, tilt angles, and

grid shifts. We retain the panel locations that are fully enclosed within the rooftop and are sufficiently from obstacles and boundaries (0.6 meters by default).

The weather files are used to generate baseline energy generation before shading for the given panel specifications, tilt options, and azimuth angle options (see 2.4.1). This computes the maximum energy each individual panel can generate. We also determine the relevant pairwise relationships between the candidate panels (geometric intersections and a time-dependent shading matrix) needed in the objective function and constraints.

The computed features are used to define the decision variables of the optimization problem, the expression for the objective function, and the constraints that require enforcement. The model inputs are defined using the Pyomo API and passed to a compatible optimization solver. We use the SBB solver to generate the results presented in this paper (except for the optimization without shading, which uses the linear solver Gurobi).



**Figure 1.** Full pipeline for rooftop solar panel optimization.

### 2.1.1. Data and User Inputs

The primary data inputs to the pipeline consist of a high-resolution satellite image and the corresponding weather file for a given region. We use 0.31-meter Worldview-3 imagery to generate all rooftop geometries using the morphological image segmentation model described in Section 2.3.1. We obtained the weather from NREL’s National Solar Radiation Database (NSRDB) [10], which provides simulated hourly radiation and weather data generated by the Physical Solar Model (PSM) Version 3. The weather files are compatible with the Python version of the System Advisor Model (PySAM) and PVWatts, which allows us to estimate the energy generation profile of a given panel over time.

The full optimization pipeline also includes several user-defined variables that can be adjusted as needed. For our default panel specifications, we use 300 W panels with dimensions of 1.6 m x 1 m with an energy generation profile modeled by the PVWatts residential profile. The default panel placement options (detailed in 2.3.2) use eight azimuth angles (in 45° intervals), four tilt angles (in 10° intervals) and four possible grid shifts (in half-panel intervals). The setback and access buffers are 0.6 m by default, based on the minimum regulatory requirement for solar PV installations in Saudi Arabia [6].

## 2.2. Optimization

### 2.2.1. Formulation

To solve for the optimal panel placement, we frame the problem as an optimal independent set problem from graph theory. An independent set refers to any subset of nodes within a graph with no mutual connections - in other words, no edge exists between any pair of nodes in the set. The maximum independent set problem is NP-complete [11], and our variation includes the added difficulty of maximizing a (potentially nonlinear) objective function rather than the number of nodes. The general form of this variation of the independent set can be represented as a constrained mixed-integer optimization problem in the form

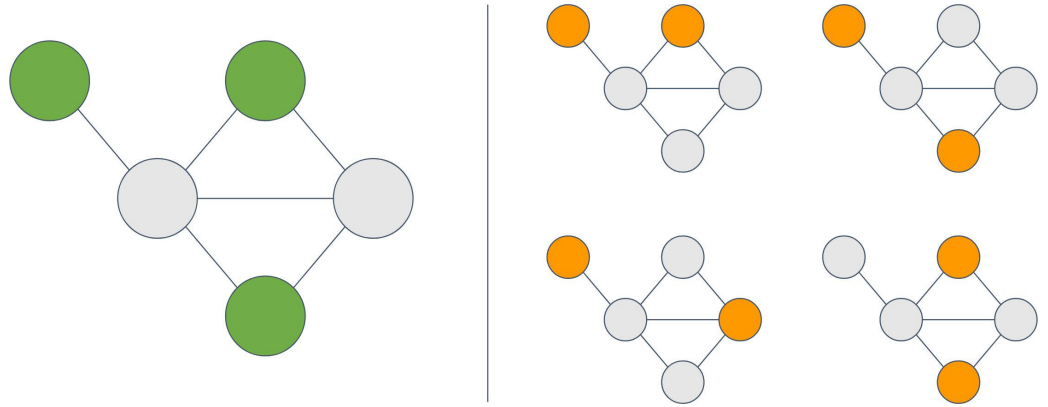
$$\begin{aligned} \max_{\vec{x}} \quad & \text{Objective}(\vec{x}, \lambda_1, \dots, \lambda_n) \\ \text{s.t.} \quad & x_i + x_j \leq 1 \quad \forall (i, j) \in E \\ & x_i \in \{0, 1\} \end{aligned} \quad (1)$$

Where the optimization method solves for the boolean vector  $\vec{x}$  (representing whether or not a candidate panel is placed) that maximizes the given objective function. The constraint enforces the requirement that, for any edge between  $(i, j)$  defined in the set of edges  $E$ , the solution can at most contain only one of the two panels. The objective function can include additional parameters  $\lambda_1, \dots, \lambda_n$  and can be arbitrarily complex in principle, but in practice it must be compatible with the optimization solver being employed.

Where the optimization method solves for the boolean vector  $\vec{x}$  (representing whether or not a candidate panel is placed) that maximizes the given objective function. The constraint enforces the requirement that, for any edge between  $(i, j)$  defined in the set of edges  $E$ , the solution can contain (at most) one of the two panels. The objective function may include additional parameters  $\lambda_1, \dots, \lambda_n$  can be arbitrarily complex in principle; however, in practice, some objective functions can present additional challenges that must be compatible with the optimization solver employed.

To formulate panel selection and layout optimization as a maximum independent set problem, we construct an intersection graph on which the nodes represent candidate panels and the edges represent a pair of panels that cannot be simultaneously placed. We define an edge between any two panels that physically overlap or that would violate placement regulations; for example, regulations related to walkways and maintenance access. However, the conditions for defining an edge can be extended to represent any binary pairwise relationship that prohibits both panels from being present simultaneously.

An independent set, in this context, represents a valid combination of panels that respects physical and regulatory constraints. The objective function we use aims to maximize the return on investment of the layout by estimating the energy generation (after shading is accounted for) over a 20-year lifetime and subtracting the estimated installation cost. This could be extended to meet household demand profiles or improved to include additional installation details, but those factors are beyond the scope of this study.



**Figure 2.** Examples of independent sets in a small graph showing (a) the maximum independent set (b) all remaining nontrivial independent sets

### 2.2.2. Objective Functions

One of the most straightforward objective functions is the weighted sum of the form in equation 2. This only requires a single additional parameter representing the panel weights, which can be selected to maximize different objectives. For example, using uniform weights maximizes the number of panels, while using the lifetime energy generation per panel maximizes the total energy generation. Similarly, by subtracting the total cost from the lifetime energy generation, this representation can also maximize a simple estimate of net return on investment when shading effects are neglected.

$$Objective(\vec{x}, \vec{c}) = \sum_{i=0}^N c_i x_i \quad (2)$$

This formulation is compatible with mixed integer linear programming (MILP) optimization solvers, which are widespread and relatively efficient when compared to nonlinear formulations. We use this formulation as a baseline to study the impact of shading losses in section 3.4, where  $\vec{c}$  is the estimated lifetime generation (neglecting shadows) minus the panel cost. However, treating each panel's energy generation independently fails to consider how panels may cast shade on each other and significantly diminish the energy generation of the final system [12].

We obtain a more realistic estimate of energy generation by incorporating a time-dependent nonlinear interaction term into the objective function. For every panel  $i$ , we compute the total area shaded by all other panels  $j$  at a specific time  $k$ . This is used to define a shading coefficient, between 0 and 1, which is multiplied by the baseline energy generation to estimate the total energy generation potential when shading effects are included.

This formulation, which involves a nonlinear objective function and a number of additional parameters, can be written as:

$$\begin{aligned} \max_{\vec{x}} \quad & \sum_{i=0}^N x_i (-C_i + T \sum_{k=0}^K G_i(k) [1 - \min(1, \sum_j x_j \cdot S_{ij}(k))]) \\ \text{s.t.} \quad & x_i + x_j \leq 1 \quad \forall (i, j) \in E \\ & x_i, x_j \in \{0, 1\} \end{aligned} \quad (3)$$



Where

- $x_i$  = A boolean decision variable that represents whether candidate panel  $i$  is selected in the solution (1 if the included in the solution, 0 if it is not)
- $N$  = The total number of candidate panels (decision variables) defined in this problem
- $K$  = The total number of unique date-time combinations considered in the energy and shading calculations
- $E$  = The set of edges in the graph representing all incompatible pairs of panels
- $G_i(k)$  = The energy generated by panel  $i$  at time  $k$  (without shading), scaled such that the sum over the  $k$  time samples equals the annual generation
- $S_{ij}(k)$  = The shaded area of panel  $i$  due to panel  $j$  at time  $k$
- $C_i$  = The marginal cost of adding panel  $i$  to the layout
- $T$  = A scaling and conversion factor that, when multiplied by the annual generation by panel  $i$ , gives the corresponding estimated lifetime financial value

(4)

In this formulation, the shading from all other selected panels  $j \neq i$  onto panel  $i$  at time  $k$  is equal to the sum of all shading contributions (representing a worst-case shading scenario). Since the energy produced cannot be negative, the total shading is capped at 1, indicating that the panel is fully shaded.

The off-diagonal terms  $S_{ij}$  (where  $i$ ) represent the shading from panel  $j$  onto panel  $i$ . The diagonal terms  $S_{ii}$  are the baseline shading of panel  $i$ , representing fixed sources of shading on  $i$  that aren't affected by any decision variables, such as nearby objects or previously placed panels in neighboring regions (which are not included in  $\vec{x}$ ).

This formulation is nonlinear and computationally demanding; as such, it is most effectively solved with specialized high-performance MINLP solvers. Smaller problems can also be recast into a form compatible with linear/quadratic solvers, such as Gurobi, by introducing additional variables and constraints. The shading coefficient can be represented by a piece-wise linear variable (to bound the coefficient between 0 and 1) with additional constraints to determine the sum over all panels.

The formulation could be further generalized to incorporate more complex real-world factors. For example, the representation in 5 uses a time-dependent tariff rate by replacing  $T$  with  $T(k)$  and absorbing it into the summation over  $K$ . This form can be used to incorporate dynamic pricing in regions where electricity prices vary based on the time of day. Additionally, since the true cost of solar installation depends on multiple nonlinear factors (including shared resources such as inverters and wiring), the constant panel cost  $C_{panel}$  can be replaced by a cost function  $C_i(\vec{x})$  that calculates the cost of adding a specific panel to a specific layout.

$$\begin{aligned}
 \max_{\vec{x}} \quad & \sum_{i=0}^N x_i (-C_i(\vec{x}) + \sum_{k=0}^K T(k) G_i(k) [1 - \min(1, \sum_j^N S_{ij}(k) x_j)]) \\
 \text{s.t.} \quad & x_i + x_j \leq 1 \quad \forall (i, j) \in E \\
 & x_i, x_j \in \{0, 1\}
 \end{aligned} \tag{5}$$

However, for the purposes of the current study, we use a fixed cost and tariff rate. This allows us to more directly evaluate the geographic and geometric characteristics of the problem without the added complexity and variability caused by incorporating time-varying local policies.

### 2.3. Site Analysis and Preprocessing

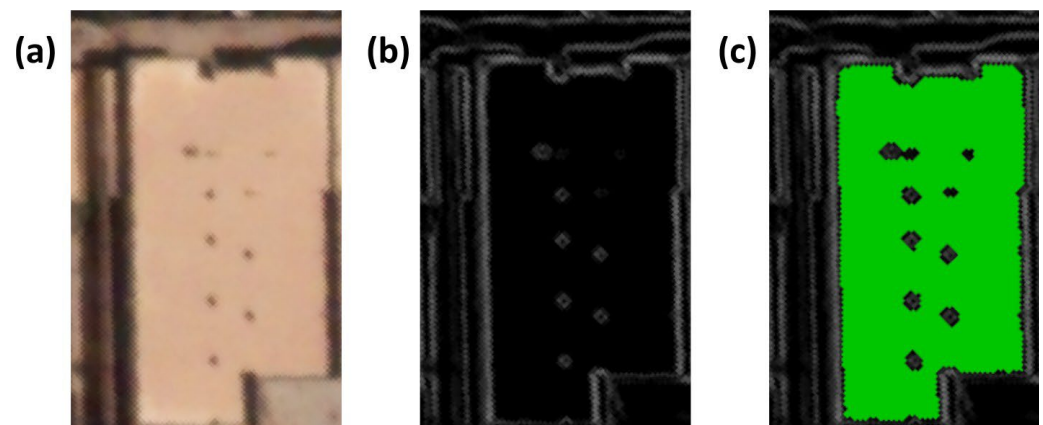
#### 2.3.1. Satellite Image Segmentation for Rooftop Detection

We identify buildings by detecting and processing edges obtained by the morphological gradient algorithm. This approach uses the difference between the dilation and erosion of a given image,  $I$ , given a kernel,  $S$ . The kernel is a small image patch used to define the neighborhood around each pixel using an image convolution. The image dilation ( $\oplus$ ) and image erosion ( $\ominus$ ) operations map each pixel to the brightest and darkest values within the kernel respectively.

$$G = I \oplus S - I \ominus S \quad (6)$$

The resulting image  $G$  is defined by the difference between the brightest and darkest pixels within the neighborhood of each pixel, as defined by the kernel  $S$ . We found the morphological gradient to be especially well suited for building application since it usually produced complete boundaries that fully enclosed objects. While alternatives such as the derivative-based Canny and Sobel detection methods are widely used for edge detection, they often produce disconnected sections of an edge with pixel-scale gaps that aren't suited to object segmentation.

A closed boundary is critical for this approach since we detect objects using the flood filling algorithm [13]. This algorithm takes a binary image and fills any holes, which are defined as regions that are enclosed within a complete internal boundary and disconnected from the outer boundary of the image. The input image is the maximum morphological gradient across all color bands, using a circular kernel with a radius of 3 pixels. The resulting image identifies all regions enclosed by a sharp change in pixel value in at least one color band, which (in our context) typically indicates different objects.



**Figure 3.** Example of rooftop detection showing a zoomed in region of (a) the RGB input image (b) morphological edge detection (c) the detected rooftop polygon with obstacles removed


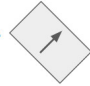

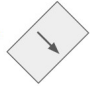

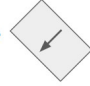

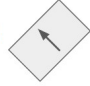







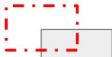
When applied to high-resolution satellite images in a dense urban setting, these objects are most often buildings, vehicles and road infrastructure. We distinguish between these objects using their geometric properties: vehicles can be filtered by their small size, and road infrastructure can be filtered by their elongated shapes [14]. We compute this by measuring the ratio of the maximum and minimum Feret diameters, which measure the largest and smallest possible separation between parallel lines that bound the object.

Optionally, to reduce misclassification and image segmentation errors, additional operations can be used to remove shadows and vegetation. Shadows are detected using the morphological shadow index (MSI) from Huang et al [15], which identifies linear morphological operators that are significantly darker than their surroundings. We also filter vegetation using NDVI, which identifies surfaces that absorb most red light but reflect most near-infrared light [16].



### 2.3.2. Candidate Panel Generation

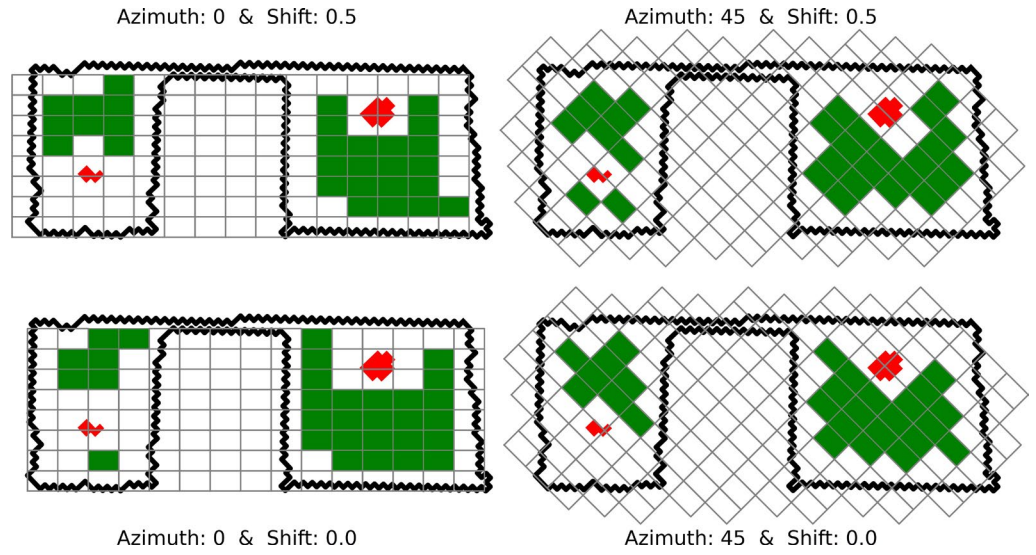
To generate the candidate panels that correspond to the set of decision variables  $\vec{x}$ , we must define their location and select one option for each of the three configuration parameters (azimuth, tilt, and shift). Using our default settings, a candidate panel has  $8 \times 4 \times 4$  possible parameter options, resulting in 128 distinct configurations before the position is taken into account. Although increasing the parameter options can improve the resolution of the state space, the combinatorial nature of these parameter choices means that increasing the options quickly becomes prohibitively expensive.

Panel Parameter	Default Set of Choices for Candidate Panels			
Azimuth Angles	0° 	45° 	90° 	135° 
	180° 	225° 	270° 	315° 
Tilt Angles	0° 	10° 	20° 	30° 
Grid Shifts				
	No shift	Horizontal shift (0.5 x panel width)	Vertical shift (0.5 x panel height)	Diagonal shift (0.5 x panel dimensions)

**Figure 4.** The default set of panel configuration options consisting of 8 possible azimuth angles, 4 possible tilt angles and 4 possible shift options

The azimuth angles and grid shifts are used to define a grid of panels, which is overlaid on the detected region (such as in figure 3c) and subsequently filtered to generate one subset of candidate panels. We require candidate panels to satisfy two key requirements: They must be fully contained within the region, and they must comply with the minimum setback requirements. Under Saudi Arabia regulations, all solar panels must be a minimum of 0.6 meters from the edge of the rooftop and any other objects. In the current study, this is achieved by applying a two-pixel buffer around all internal and external boundaries in the rooftop geometry.

The azimuth angles and grid shifts are used to define a grid of panels, which is overlaid on the detected region (see figure 3c) and then filtered to generate one subset of candidate panels. We require any candidate panels to satisfy two key requirements: they must be fully contained within the region, and they must comply with the minimum setback requirements. Regulations in Saudi Arabia require that all solar panels are a minimum of 0.6 meters away from the edge of the rooftop and from any objects, which is implemented by applying a 2-pixel buffer (corresponding to 0.61 meters) around all internal and external boundaries in the rooftop geometry.



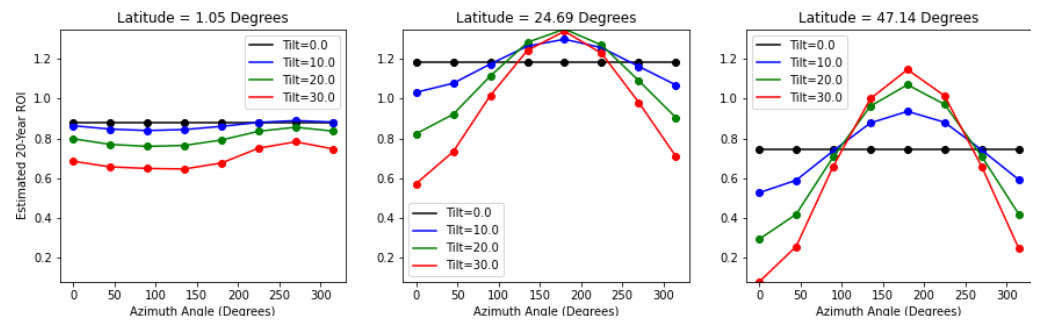
**Figure 5.** Examples of different panel grids (gray) overlaid on a detected building polygon (black) with obstacles (red). The panels that satisfy all placement requirements (shown in green) are viable candidate panels and are included as decision variables

Each of these candidate panels is assigned a baseline energy generation, as defined in section 2.4.1, based on its azimuth and tilt angle. Additionally, for all pairs of panels included in a set of decision variables  $\tilde{x}$ , we compute the pairwise shading terms  $S_{ij}(k)$  and  $S_{ji}(k)$  as defined in sections 2.4.2 and 2.4.3.

## 2.4. Energy Estimation

### 2.4.1. Baseline Energy Generation

Each candidate panel has a defined photovoltaic module, azimuth angle (which defines the compass direction of the surface normal) and tilt angle relative to a flat ground surface. We provide these parameters and the corresponding weather file into PySAM to estimate the baseline energy generation for every snapshot time. We used one year of hourly weather data for all of the locations in this study.



**Figure 6.** Resulting 20-year return on investment (ROI) for a single panel based on PySAM generation profiles for the three study regions at different latitudes, shown for different panel tilts and azimuth angles, when computed using the default panel cost and tariff rate.

These results provide the baseline energy generation for an unshaded panel for different times of day and different days of the year. These are combined with the shaded area of the panel to compute the final energy generation.

To incorporate the baseline energy generation profile into the objective function, we generate a small representative subset of the year by using the 14th day of each month and only considering major daylight hours (6 am to 8 pm in the local time zone). These

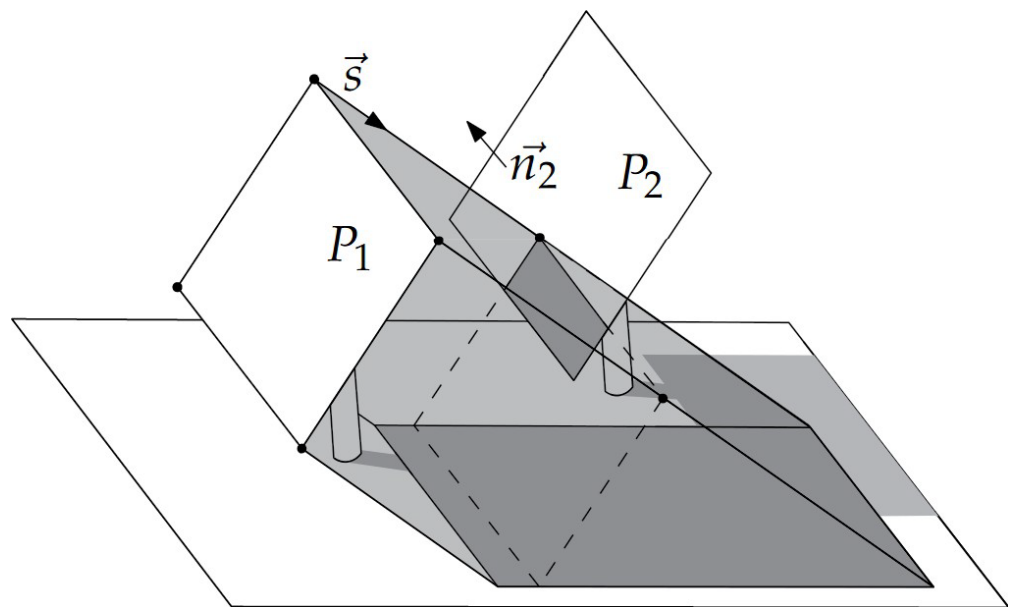
combinations provide a total of 168 time samples during significant daylight hours, which are scaled by 365/12 to recover the approximate annual energy generation. Since they are distributed approximately evenly across all seasons, they reasonably characterize the different shading conditions experienced in a typical year.

#### 2.4.2. Panel Shading

Photovoltaic panels are highly sensitive to shading in multiple respects. The most immediate effect is the reduction in energy generation, which can have a complicated nonlinear relationship with area being shaded [12]. In the long term, nonuniform energy generation (both among different solar cells within a panel, and different solar panels connected to the same inverter) can significantly accelerate panel degradation. Although partial shading is difficult to avoid entirely, we reduce their impact by penalizing energy losses due to shading in the objective function.

We model the shading caused by panels using the shadow volume algorithm, one of the oldest and most common techniques for 3D shadow rendering [17]. This creates 3D volumes to represent shadows cast by objects and separate 3D space into two regions: all surfaces inside the volume is shaded, and all surfaces outside are not shaded by this object. In the case of a rectangular photovoltaic panel, the shadow volume takes the form of an oblique parallelepiped extending from the panel vertices on surface ( $P_1$ ) in the direction of the unit vector  $\vec{s}$  representing the direction of sunlight (the azimuth and elevation angles) at that geographic location and the given time and date.

To compute the resulting shading on panel  $P_2$  due to  $P_1$ , we need determine the intersection of the shadow volume of  $P_1$  with the surface of panel  $P_2$ . This is computed in two stages, using the geometric setup shown in figure 7. The first determines the intersection of the shadow volume of  $P_1$  on the infinite surface plane defined by  $P_2$ . If such an intersection exists, we proceed to the next step to determine how much of the panel is shaded (otherwise, there is no shading by  $P_1$  on  $P_2$  at this location at this time).



**Figure 7.** An example of the shading between two nearby panels at a single point in time, showing the shadow volume as a 3D parallelepiped and the shaded region as a dark gray quadrilateral on panel  $P_2$

If an intersection exists between the 3D shadow volume of  $P_1$  and the 2D infinite plane containing  $P_2$ , there is a possibility that  $P_2$  experiences shading due to  $P_1$ . The final step is to determine the intersection within the boundaries panel  $P_2$ , which we accomplish using a change of basis to the intersection plane to reduce the problem to 2 dimensions. This

allows us to obtain the final shaded area by computing the 2D intersection of two polygons: one representing the panel  $P_2$ , and the other representing the intersection of the shadow volume of  $P_1$  with the infinite plane of  $P_2$ .

### 2.4.3. Shadow Matrix

The shaded area computed in section 2.4.2, divided by the total area of the panel, represents the fractional shaded area on  $P_2$  due to  $P_1$  (and is approximately proportional to the energy loss). Before running the optimization, we precompute all pairwise shading terms and store them in the shadow matrix element  $S_{ij}(k)$  (where  $i$  and  $j$  are the indices of panels  $P_2$  and  $P_1$  respectively, and  $k$  corresponds to the date-time pair being evaluated). This structure allows us to incorporate accurate pairwise shading in 3D space between two panels with arbitrary azimuth and tilt angles.

Additionally, this representation allows us to incorporate fixed sources of shading that aren't affected by the decision variables. This is stored in the matrix diagonal  $S_{ii}(k)$ , and acts as a baseline shading term that always affects panel  $i$ . In principle, this can be used to represent any fixed sources of shading such as nearby walls, neighboring buildings and other rooftop objects. In our implementation we use it to account for shading from previously placed panels in nearby regions, which contributes additional shading that can affect subsequent layouts.

One limitation of this implementation is that each pairwise shading term is computed individually, and shading from multiple panels is added linearly to get the total shaded area. Computing the exact combined shading from all panels would be too computationally prohibitive to include in the objective function. This represents the worst-case scenario where all shaded areas are non-overlapping, which may overestimate the total shaded area in cases of heavy shading.

## 2.5. Implementation and Performance

### 2.5.1. Sequential Optimization

Due to the computational complexity of MINLP optimization, and the highly combinatorial nature of the candidate panel generation defined in 2.3.2, solving a full rooftop in a single optimization may require prohibitively large amounts of RAM. In such cases, we use polygon decomposition to segment the rooftop into multiple regions that can be optimized sequentially. By limiting the maximum number of candidate panels in each segment (600 by default), we can optimize a rooftop in batches that place a hard limit on the size of the individual optimization runs.

To define the initial polygon segments, we use a network-based community detection approach to identify regions with clusters of high mutual visibility. In computational geometry, a pair of 2D points are visible to one another if a straight line between them does not intersect with any polygon boundaries. We use this to define a visibility network, where nodes represent points along the perimeter and edges identify pairs of points that are visible to one another. These are clustered using the Walktrap algorithm in Python's *igraph* library [18] to identify regions of high visibility.

The resulting regions are typically separated by obstructions or bottlenecks in the polygon, since these would obstruct visibility between two adjacent regions. If any of these initial segments still contain more candidate polygons than the user-defined limit, they are further segmented through iterative bisection. After identifying the minimum rotated bounding box, we split the polygon into two using a bisection connecting the midpoints of the two long sides of the rectangle. This bisection procedure is repeated for any remaining polygon segments that exceed the candidate panel limit.

To perform sequential optimization while accounting for shading interactions between regions, we treat all previously placed panels as fixed sources of shading for subsequent sets of candidate panels (as defined in section 2.4.3). We use multiple sweeps along the sequence (2 by default) to allow earlier placements to be improved in response to shading from panels that were placed after. Although this approach will not generally give the same

solution as a single large optimization, it enables greater scalability of MINLP geometric optimization since it can support arbitrarily large polygons while limiting maximum RAM usage.

### 2.5.2. Hardware Specifications

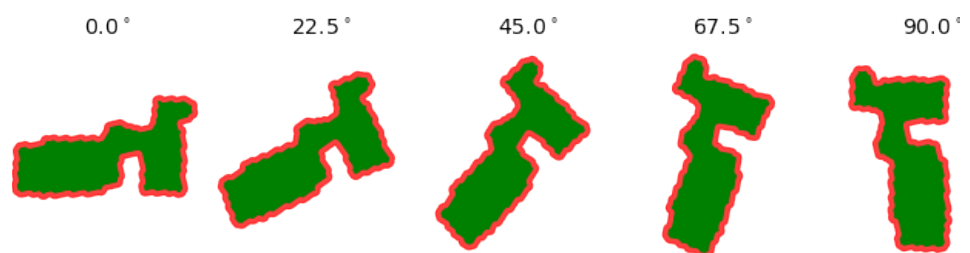
The shading analysis and optimization represent the bulk of the running time, and were executed on a desktop PC equipped with an Intel Core i7 12700k CPU (base clock: 3.6 GHz, boost clock: up to 5 GHz) and 128 GB of DDR4 RAM. Due to limitations on the RAM usage by the optimization solver, we used batch sizes of 600 candidate panels or less by default for the full MINLP problem in 3. The running time for each building was highly variable, increasing with the total number of candidate panels, but a typical rooftop in our data set would complete the shadow matrix calculation and the layout optimization in a total of 10 to 20 minutes.

## 3. Results

### 3.1. Regions of Study

To extract rooftop geometries, we used 0.31 meter Worldview-3 satellite images of a typical residential neighborhood in Riyadh, Saudi Arabia. These geometries can be artificially reassigned to any latitude, as long as the corresponding weather file is available. By using the same rooftop geometries in different regions, we can isolate the impact of generation potential and shading losses on the generated layouts.

In addition to our initial study region of Riyadh, Saudi Arabia (approximately 25° latitude, 48 longitude), we performed the same analysis in central Washington state (approximately 47 latitude and -120 longitude) and northern Brazil (approximately 1 latitude, -54 longitude). These regions were selected due to their weather history and nearly even spacing across latitudes. Central Washington is relatively dry and has nearly the same peak solar energy potential as Riyadh, making it well suited for comparative analysis. Due to limited availability of SAM-compatible weather data at lower latitudes, we selected Brazil even though it exhibits less solar potential overall (approximately 35% lower annual generation for the highest performing panels).



**Figure 8.** An example of a detected building rotated to the 5 default alignments

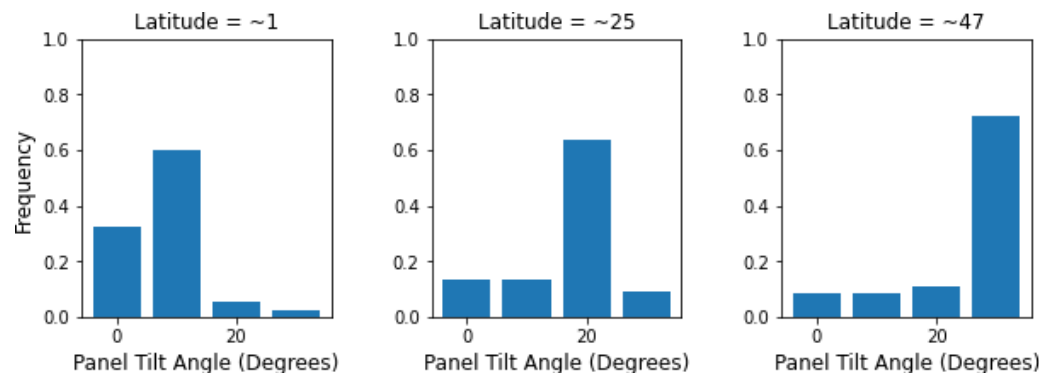
To explore the role of urban planning and solar efficiency, we also vary the rotation angle of the rooftop geometries. We define the orientation of the principal axis as the longest side of the minimum rotated bounding box enclosing the polygon. Rotation angles are relative to the equator, where a rotation angle of 0° aligns the longest side of the bounding box to the horizontal axis (maximizing the width of the rooftop). We analyze rotations between 0° and 90°, in intervals of 22.5°, to evaluate how urban layouts may impact rooftop solar potential.

Our primary variables relating to panel configuration are the panel azimuth angle (where 0° is north-facing and 90° is east-facing) and the tilt angle (where 0° is parallel to the ground and 90° is perpendicular). We will explore potentially general design characteristics by examining statistical differences for different regions and rotation angles.



### 3.2. Effect of Latitude on Panel Configurations

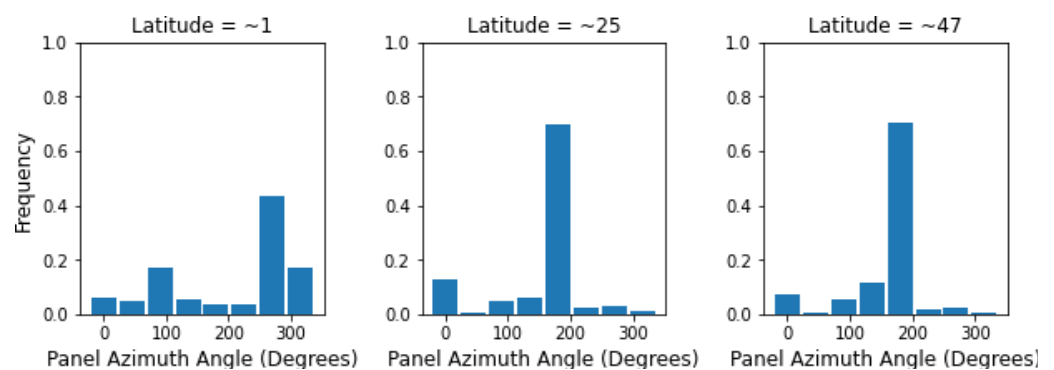
The tilt angles in the optimized layouts are generally consistent with the highest-performing choices in figure 6. For moderate and high latitudes, this led to the highest performing tilt angle to represent approximately 70% of the solution. Near the equator, the situation is slightly more complex since the two lowest tilt angles both achieve comparable performance: there is slight preference for  $10^\circ$  for partially or fully west-facing panels, and a preference  $0^\circ$  for all other azimuth angles. As a result, the solutions feature a mixture of the two tilt angles with a preference for  $10^\circ$  overall since they allow for slightly higher performance.



**Figure 9.** The frequency of selected tilt angles for solutions at different latitudes

Remaining tilt angles occur in small quantities, which could occur for a variety of reasons. The rate of 10–15% (for moderate to high latitudes) may result from trying to avoid shading losses, since low tilts cause less shading and high tilts are less susceptible to shading. In specific cases, this may incentivize the use of lower-performing panels if they lead to reduced shading losses. Additionally, this may reflect characteristics of a locally optimal solution since MINLP problems have high computational complexity and solvers typically cannot guarantee global optimality.

Similarly, with azimuth angles we see a very strong preference for the highest performing panel configurations shown in figure 6. Away from the equator, approximately 70% of panels are south-facing and the remaining azimuth angles are present in small quantities. A notable exception is north-facing panels at  $25^\circ$  latitude, which appear more often than some higher ROI configurations. Since these conveniently fit behind south-facing panels without shading losses (for equal tilt angles), they can be used to fill in small gaps where panels with a higher individual ROI may suffer from higher shading losses or might not fit at all (due to spacing and access regulations).



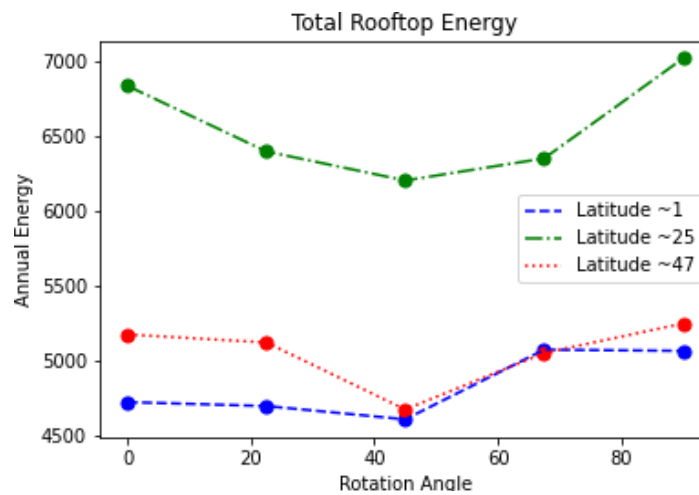
**Figure 10.** The frequency of selected azimuth angles for solutions at different latitudes

Near the equator, at least based on the weather profile in the Amapa region of Brazil, there is a preference for west-facing panels consistent with the maximum ROI configuration

shown in figure 6 for tilt angles of  $10^\circ$ . As before, we see a second peak at the opposite azimuth angle of the main peak. Since east-facing panels can be placed directly behind west-facing ones and face little or no shading losses, they are a geometrically convenient way to fill gaps that wouldn't permit or reward panels that have a higher baseline generation.

### 3.3. Impact of Building Rotation

To examine the effects that urban planning can have on rooftop solar energy potential (with a particular focus on parcel layout), we artificially rotate the building to align its principal axis to one of 5 rotation angles ranging from  $0^\circ$  (horizontal) to  $90^\circ$  (vertical). Figure 11 shows how the energy generation potential changes depending on the rotation angle for each latitude.



**Figure 11.** The total annual energy generated, as an average across all tested rooftops, for different degrees latitude, as a function of the building rotation angle

For medium and high latitudes, we can see that the  $0^\circ$  (horizontal) to  $90^\circ$  (vertical) rotation angles consistently outperform the rest, and for all latitudes the  $45^\circ$  angle consistently produces the least energy. The equatorial case is the only result where the  $0^\circ$  building exhibits notably weak performance, which may be a consequence of its unique shading properties. Since shading near the equator is almost entirely along the east-west axis, the horizontal alignment would be the most susceptible to shading losses, and a vertical or near-vertical alignment would be the least susceptible.

In principle, this could be caused by a number of causes that may either be general to the problem or specific to the formulation. These include panel efficiencies, shading effects and discretization of the solution space (which can affect the maximum geometric capacity). Although we can't fully decouple these potential causes from the results of the optimization, we can obtain some insight by exploring the role of shading effects and how they impact the efficiency of resulting panel configurations.

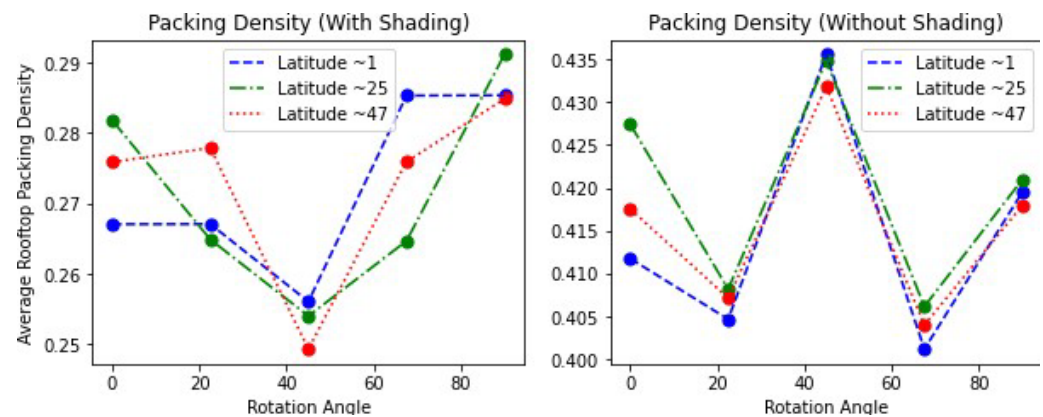
### 3.4. Impact of Shading Losses

In general, the average shading losses tend to remain low (an average of 1-3% loss for all latitudes and rotation angles) even though individual panels in the solution sometimes exhibit shading losses as high as 20% (or even 30% at high latitudes). This suggests that although significant shading losses do not necessarily eliminate a candidate panel from selection, they appear to be strongly disincentivized in nearly all cases and rarely selected by the optimization solver in practice.

We can examine the effect of shading on the optimization by comparing the packing density for the full optimization with shading (as defined in 3) with a simplified variant that has all shading disabled, which can be reduced to the form 2, with appropriate choice

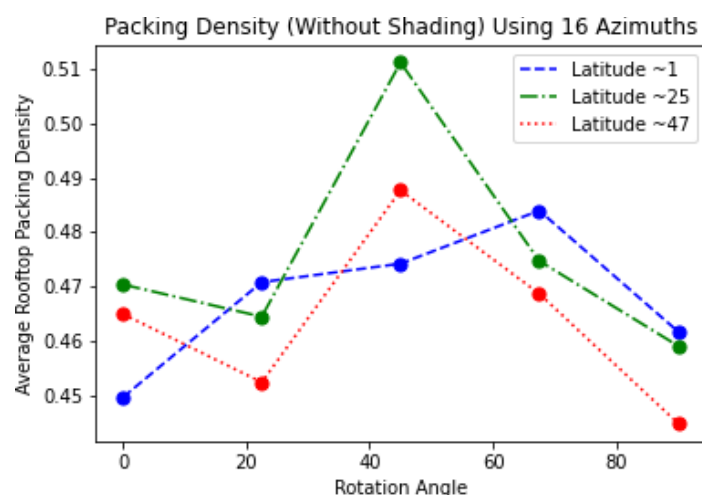
of the weights  $C_i$ . These result in a number of changes to the resulting layouts and panel characteristics.

When shading is included, the resulting layouts have the highest generation packing density when the buildings have a principal axis along or near the horizontal ( $0^\circ$ ) or vertical ( $90^\circ$ ) rotation angles. These building alignments represent the "wide" and "tall" orientations of a given rooftop, and can most easily support simple parallel row arrangements with low shading losses. The  $45^\circ$  alignment, however, consistently exhibits the lowest packing density for all latitudes when shading is included.



**Figure 12.** The packing density (ratio of panel area to rooftop area) of solutions to the shaded (left) and unshaded (right) optimization formulations

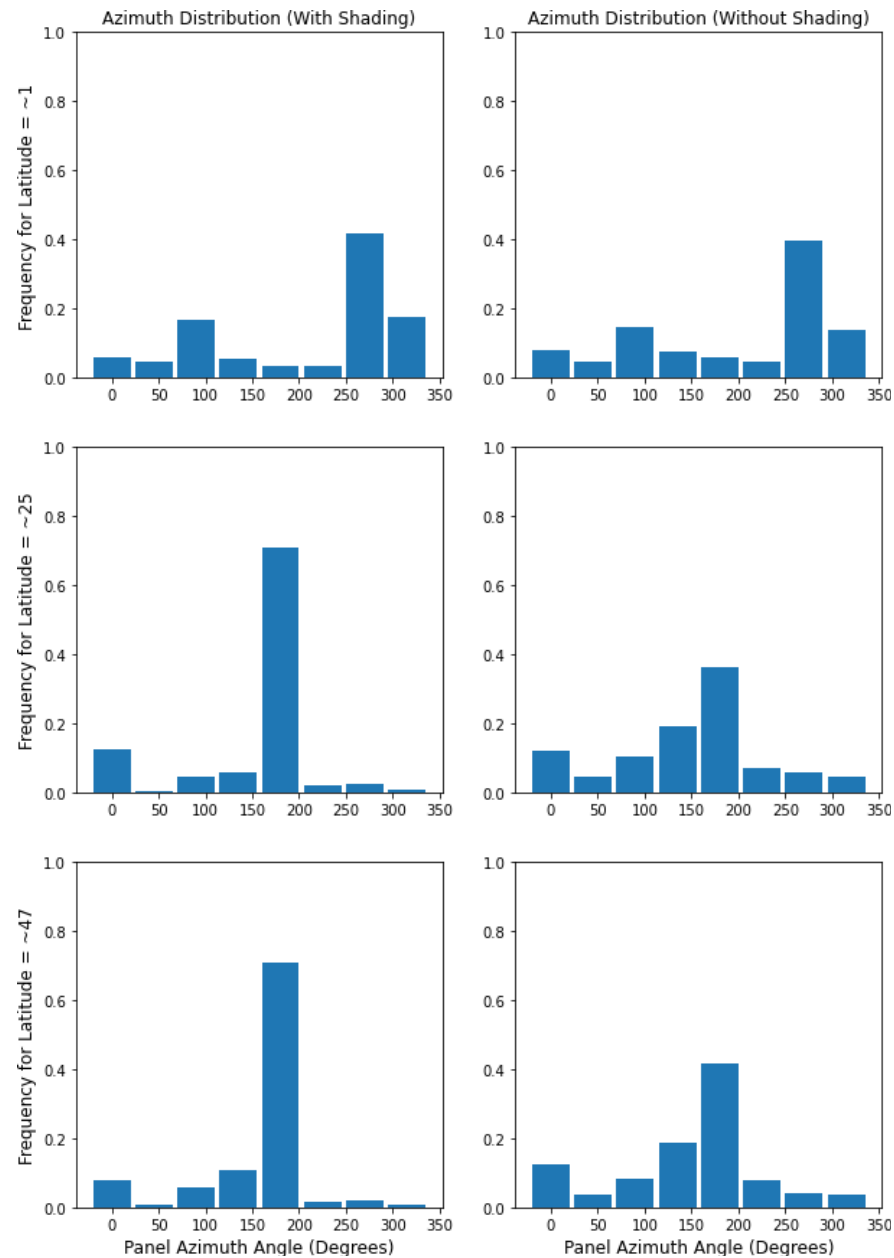
In contrast, in the solutions to the optimization without shading the  $45^\circ$  alignment consistently outperforms all other building rotation angles at every tested latitude. This result suggests that, unlike the  $22.5^\circ$  and  $67.5^\circ$  alignments, the  $45^\circ$  alignment tends to have an advantage in terms of geometric capacity. Since the  $22.5^\circ$  and  $67.5^\circ$  alignments are not parallel to any of the 8 default panel azimuths, they consistently have the lowest packing density, but this disadvantage no longer exists when the panel azimuth options are increased to avoid that limitation (figure 13).



**Figure 13.** The average packing density, after doubling the possible azimuth angles to 16, for solutions to the unshaded optimization problem

However, despite its high geometric capacity the  $45^\circ$  alignment appears to be the least capable of effectively utilizing the available space when shading effects are included. Comparing the choice of azimuth angles (figure 14) for the two cases can help shed some

light on the driving factors behind these differences. When the optimization is performed without shading, we can see that higher latitudes are significantly more likely to use a variety of azimuth angles to achieve a higher packing density. Although the individual panels have a lower average baseline energy generation, this is outweighed by the increase in panel count when interaction effects are neglected.



**Figure 14.** The distribution of panel azimuth angles in solutions to the shaded (left) and unshaded (right) optimization formulations at different latitudes

In combination, these results suggest that panel shading interactions play a crucial role in the design of effective rooftop PV layouts, and can have different effects depending on the latitude of the site. Without shading, the optimized solutions tend to prioritize high density over individual panel performance. When shading is included, the most effective layouts at higher latitudes are often dominated by a single azimuth angle with high individual panel generation (with a tendency to form spaced rows), using a mix of other panel configurations in small quantities to fill in gaps without substantially increasing the average shading loss.

## 4. Discussion

The methodology presented in this paper demonstrates the potential of image processing and MINLP optimization methods to evaluate rooftop solar energy potential and layout design. The results suggest that shading interactions play a critical role in the design choices of optimized layouts, particularly at locations far from the equator. The results suggest that although single-azimuth equator-facing row layouts are an effective rule of thumb for greater latitudes, overall performance improves by multi-azimuth layouts that primarily (but not exclusively) follow an equator-facing row structure.

In addition to using the generating PV layouts directly for building-level site assessment and energy projection, this methodology also suggests that urban planning and building geometry may play an important role in the performance of residential rooftop PV installations. In particular, building alignment (which is typically parallel to adjacent road and parcel boundaries) seems to affect layout performance significantly. This effect appears to be driven by shading interactions.

There are several potential opportunities for further research, encompassing improvements to the optimization and extensions to the analysis. Alternate formulations might be able to avoid the limitations caused by the discretized panel configurations in our approach. Additionally, further work is needed to establish the relationship between urban planning choices (particularly how they affect building geometry) and the efficacy of rooftop PV layouts at greater latitudes.

### 4.1. Residential PV Layout Design

The results of our optimization methodology demonstrate a few key characteristics (when shading effects are included) that suggest or verify general best practices for PV layout design. They suggest that the common approach of using single-azimuth layouts tends to be effective in cases where they are geometrically viable (e.g. solar farms and large, open rooftops) but can often be improved by allowing additional azimuth angles. Although these non-primary azimuth angles have lower baseline energy capacities, they increase the overall generation by filling in gaps in irregular geometries without substantially increasing shading losses.

However, the comparison of results different latitudes suggests that these best practices are not universal and differ significantly between equatorial and non-equatorial regions. The average distribution of azimuth angles is dominated by equator-facing panels (approximately 70%) at greater latitudes, but only exhibit a modest preference (approximately 40%) towards the highest-performing azimuth angle for equatorial regions. In non-equatorial regions, the optimized solutions tend to feature single-azimuth rows, while solutions near the equator tend to result in less structured arrangements.

### 4.2. Building Geometry and Urban Planning

In addition to comparing results at different latitudes, altering the alignment of a building's principal axis (relative to the equator) allows us to examine the role that urban planning might play in renewable energy adoption. Since building alignments are typically parallel to road and parcel layouts, it may provide an opportunity for policymakers to help increase the solar generation potential of residential rooftops. Our results suggest that buildings that are primarily parallel or perpendicular to the equator are the most effective, with results that vary slightly by latitude.

At greater latitudes, the highest performing rooftops tended to be approximately parallel or perpendicular to the equator ( $0^\circ$  or  $90^\circ$ ). In contrast, the  $45^\circ$  alignment consistently produced the least energy and contained the fewest panels. Comparing this with the shadow-free optimization (figure 12) indicates that this is driven primarily by shading effects rather than geometric characteristics. Near the equator, however, shading is directed almost entirely along the east-west axis so the vertical and near-vertical alignments exhibit the best performance for the optimization with shading. Since the vertical alignment mini-



mizes the width of the rooftop polygon, it appears to be the most effective layout to reduce shading effects.

Urban planners and policymakers might be able to increase residential rooftop PV adoption and generation potential by establishing guidelines for solar-friendly building designs. The results in this paper suggest that horizontally and/or vertically aligned buildings tend to produce the highest output, depending on the degree latitude, but only when shading effects are accounted for. Future research into the sensitivity to building alignment and other geometric characteristics could be of interest to urban planners, architects and government officials.

#### 4.3. Evaluating Common Design Heuristics

Based on the results shown in sections 3.2, 3.3 and 3.4, the optimized layouts exhibit patterns that appear broadly consistent with the common design heuristics reviewed in section 1.2.2. However, we see a sensitivity to both latitude and shading effects that should be taken into consideration when applying these heuristics. Additionally, we can see where our more general layout generation method breaks these patterns to improve performance.

The first heuristic described in 1.2.2, which encourages using equator-facing panels at a specific tilt angle, seems effective at higher latitudes but less significant near the equator. For latitudes  $25^\circ$  and  $47^\circ$ , around 70% of panels were south-facing in the final optimized layouts (typically at, or near, the highest performing tilt angle). Interestingly, this pattern was not prominent when we excluded shading interactions, suggesting that shading effects may be at least partially responsible for the efficacy of this heuristic. Without shading effects, the optimization method uses a more diverse mix of azimuth angles to prioritize high packing density instead.

The second heuristic, which recommends using spaced row layouts, is also consistent with the results when shading interactions are included. This partially follows from the previous case (the preference for equator-facing panels) but also relies on the ability of spaced rows to minimize shading interactions. When we exclude shading effects, the optimized layouts are much denser and seldom feature row structures. As before, this heuristic primarily matched the results at higher latitudes and did not appear to be significant near the equator.

In contrast, the third heuristic (to align panels to building geometry) appears to become considerably less useful when shading interactions are included, at least for the rooftops examined in this study. This design pattern seems to emerge only when we neglect shading losses (see figure 12) and disappears when shading losses are included. This suggests that this heuristic may be ineffective in cases where shading interactions are significant, even if it can be a helpful rule of thumb in more generic packing problems (such as layout optimization without shading).

The first two heuristics seem to emerge from shading interactions, and are consistent with around 70% of the panels present in the optimized layouts. In contrast, the third heuristic only appears when shading effects are neglected, suggesting that it is ineffective in this context even if it is helpful in more general packing problems. Although the third heuristic allows for increased packing density, it likely suffers from increased shading losses as well. These observations support using heuristics that prioritize high individual panel outputs and low shading losses, but not heuristics that increase packing density.

#### 4.4. Limitations and Future Work

There are several built-in assumptions in the formulation that affect the solutions, and should be kept in mind when interpreting these results. The spacing and access regulations in Saudi Arabia (such as a 60 cm minimum buffer in front of every panel) certainly contribute to the tendency towards spaced row structures. In regions without such restrictions, spaced rows would likely be outperformed by dense flat layouts without spacing (with 0 tilt to eliminate shading interactions). Additionally, the discrete panel configuration choices (azimuth, tilt and location) introduce discretization error and lead to

a combinatorial explosion in the number of decision variables, which limits the parameter-space resolution.

Additionally, the solutions (for nonlinear and non-convex objective functions) are not guaranteed to be globally optimal. Further research into alternate formulations and solvers may help improve the performance of the final solutions, and comparative studies between different formulations may shed light on the specific properties suggested in our results.

## 5. Conclusions

Throughout this paper, we demonstrate the successful implementation of multi-azimuth PV layout optimization with shading interactions. The results suggest that a combination of azimuth angles often outperform single-azimuth designs for flat residential rooftops with obstructions. We also saw that shading losses played a large role in layout design, with markedly different effects near the equator compared to higher latitudes.

Additionally, we evaluated several heuristics by identifying patterns in the optimized results (with and without shading). Our results also suggest that heuristics that improve packing density may not be useful when shading interactions are included. In contrast, heuristics that reduce shading losses (such as equator-facing panels and spaced rows) are consistent with optimized layouts and appear to emerge naturally in the context of shaded PV optimization.

Since there is limited existing research that uses MINLP for nonlinear PV layout optimization with partial panel shading, there are several potential avenues for future research. Different formulations may be more computationally efficient or generate higher-performance layouts. Alternatively, there may be more effective optimization solvers that can find better solutions for nonlinear, non-convex objectives.

**Author Contributions:** Conceptualization, Z.A., A.A., and A.H.; methodology, Z.A. and A.A.; software, Z.A. and A.A.; validation, Z.A., A.A., and A.H.; formal analysis, Z.A.; investigation, Z.A.; resources, Z.A.; data curation, Z.A.; writing—original draft preparation, Z.A. and A.A.; writing—review and editing, Z.A., A.A., A.H. and O.W.; visualization, Z.A.; supervision, A.H. and O.W.; project administration, A.H. and O.W.; funding acquisition, A.H. and O.W. All authors have read and agreed to the published version of the manuscript.

**Funding:** This research was funded by the King Abdulaziz City for Science and Technology (KACST)

**Data Availability Statement:** In this section, please provide details regarding where data supporting reported results can be found, including links to publicly archived datasets analyzed or generated during the study. Please refer to suggested Data Availability Statements in section "MDPI Research Data Policies" at <https://www.mdpi.com/ethics>. If the study did not report any data, you might add "Not applicable" here.

**Acknowledgments:** This research was supported by project funding and commercial satellite data provided by the King Abdulaziz City for Science and Technology (KACST)

**Conflicts of Interest:** The authors declare no conflict of interest.

## References

1. Alice Detollenaere, G.M. *Snapshot of Global PV Markets 2021*; International Energy Agency, 2021.
2. Guittet, D.L.; Freeman, J.M. *Validation of Photovoltaic Modeling Tool HelioScope Against Measured Data*; National Renewable Energy Laboratory.
3. Zhong, Q.; Nelson, J.R.; Tong, D.; Grubescic, T.H. A spatial optimization approach to increase the accuracy of rooftop solar energy assessments. *Applied Energy* **2022**, *316*, 119128. <https://doi.org/10.1016/j.apenergy.2022.119128>.
4. Narjabadifam, N.; Al-Saffar, M.; Zhang, Y.; Nofech, J.; Cen, A.C.; Awad, H.; Versteeg, M.; Gül, M. Framework for Mapping and Optimizing the Solar Rooftop Potential of Buildings in Urban Systems. *Energies* **2022**, *15*. <https://doi.org/10.3390/en15051738>.
5. Gagnon, P.; Margolis, R.; Melius, J.; Phillips, C.; Elmore, R. *Rooftop Solar Photovoltaic Technical Potential in the United States: A Detailed Assessment*; National Renewable Energy Laboratory, 2016.
6. *Regulations on the installation of Solar Panels on Buildings and Facilities (Title Translated from Arabic)*; Saudi Arabian Ministry of Municipal and Rural Affairs, 2021.
7. Al-Quraan, A.; Al-Mahmodi, M.; Alzaareer, K.; El-Bayeh, C.; Eicker, U. Minimizing the Utilized Area of PV Systems by Generating the Optimal Inter-Row Spacing Factor. *Sustainability* **2022**, *14*. <https://doi.org/10.3390/su14106077>.

8. Feng, Y.T.; Han, K.; Owen, D.R.J., An Advancing Front Packing of Polygons, Ellipses and Spheres. In *Proceedings of the Third International Conference on Discrete Element Methods: Numerical Modeling of Discontinua*; pp. 93–98. [https://doi.org/10.1061/40647\(259\)17](https://doi.org/10.1061/40647(259)17).
9. Pasha, A. Geometric Bin Packing Algorithm for Arbitrary Shapes. Master's thesis, University of Florida, 2003.
10. Sengupta, M., Y.X.A.L.A.H.G.M.; Shelby, J. The National Solar Radiation Data Base (NSRDB). *Renewable and Sustainable Energy Reviews* **2018**, *89*, 51–60.
11. Baker, B.S. Approximation Algorithms for NP-Complete Problems on Planar Graphs. *J. ACM* **1994**, *41*. <https://doi.org/10.1145/174644.174650>.
12. Meyers, B.; Mikofski, M. Accurate Modeling of Partially Shaded PV Arrays. In *Proceedings of the 2017 IEEE 44th Photovoltaic Specialist Conference (PVSC)*, 2017, pp. 3354–3359. <https://doi.org/10.1109/PVSC.2017.8521559>.
13. Soille, P. *Morphological Image Analysis: Principles and Applications*, 2nd ed.; Springer-Verlag, 1999; pp. 173–174.
14. Awwad, Z.; Alnasser, F.; Alshahrani, T.; Moraguez, M.; Alabdulkareem, A.; de Weck, O. Self-Supervised Deep Learning for Vehicle Detection in High-Resolution Satellite Imagery. In *Proceedings of the 2021 IEEE International Geoscience and Remote Sensing Symposium IGARSS*, 2021, pp. 2337–2340. <https://doi.org/10.1109/IGARSS47720.2021.9554580>.
15. Huang, X.; Zhang, L. Morphological Building/Shadow Index for Building Extraction From High-Resolution Imagery Over Urban Areas. *IEEE Journal of Selected Topics in Applied Earth Observations and Remote Sensing* **2011**.
16. Tucker, C.J. Red and photographic infrared linear combinations for monitoring vegetation. *Remote Sensing of Environment* **1979**, *8*, 127–150.
17. Crow, F.C. Shadow Algorithms for Computer Graphics. In *Proceedings of the ACM SIGGRAPH 1977 Proceedings*, 1977, Vol. 11, p. 242–248.
18. Pons, P.; Latapy, M. Computing Communities in Large Networks Using Random Walks. In *Proceedings of the Computer and Information Sciences - ISCIS 2005*; Yolum, p.; Güngör, T.; Gürgeç, F.; Özturan, C., Eds.; Springer Berlin Heidelberg: Berlin, Heidelberg, 2005; pp. 284–293.